AD-A092 274 WEIDLINGER ASSOCIATES NEW YORK F/G 8/7

GROUND SHOCK ON ALLUVIAL GEOLOGIES. STUDY OF THE EFFECT OF CEME--ETC(U)

JUN 80 I S SANDLER, D RUBIN DNA001-77-C-0035

UNCLASSIFIED DNA-5253F NL

END

DATE FILMED

1 81

DTIC

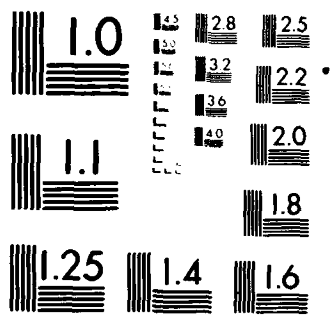

MICROCOPY RESOLUTION TEST CHART
NATIONAL BUREAU OF STANDARDS 1963 A

LEVEL II

DNA 5253F

GROUND SHOCK ON ALLUVIAL GEOLOGIES

Study of the Effect of Cementation Breakdown and Pore Air Phenomena

AD A092274

Weidlinger Associates
110 East 59th Street
New York, New York 10022

30 June 1980

Final Report for Period 20 October 1976—30 June 1980

CONTRACT No. DNA 001-77-C-0035

THIS WORK SPONSORED BY THE DEFENSE NUCLEAR AGENCY
UNDER RDT&E RMSS CODE B344079464 Y99QAXSB27707 H2590D.

Prepared for
Director
DEFENSE NUCLEAR AGENCY
Washington, D. C. 20305

UNCLASSIFIED

SECURITY CLASSIFICATION OF THIS PAGE (When Data Entered)

REPORT DOCUMENTATION PAGE

19

READ INSTRUCTIONS BEFORE COMPLETING FORM

1. REPORT NUMBER: DNA 5253F (18)

2. GOVT ACCESSION NO.: AD-A092 274

3. RECIPIENT'S CATALOG NUMBER: (9)

4. TITLE (and Subtitle): (6) GROUND SHOCK ON ALLUVIAL GEOLOGIES. Study of the Effect of Cementation Breakdown and Pore Air Phenomena.

5. TYPE OF REPORT & PERIOD COVERED: Final Report, for Period 20 Oct 76—30 Jun 80

6. PERFORMING ORG. REPORT NUMBER

7. AUTHOR(s): (10) Ivan S. Sandler, David Rubin

8. CONTRACT OR GRANT NUMBER(s): (15) DNA 001-77-C-0035

9. PERFORMING ORGANIZATION NAME AND ADDRESS: Weidlinger Associates, 110 East 59th Street, New York, New York 10022 (12) 44

10. PROGRAM ELEMENT, PROJECT, TASK AREA & WORK UNIT NUMBERS: Subtask Y99QAXSB277-07 (16)

11. CONTROLLING OFFICE NAME AND ADDRESS: Director, Defense Nuclear Agency, Washington, D.C. 20305 (11)

12. REPORT DATE: 30 Jun [redacted] 80 (17)

13. NUMBER OF PAGES: 44

14. MONITORING AGENCY NAME & ADDRESS (if different from Controlling Office)

15. SECURITY CLASS (of this report): UNCLASSIFIED

15a. DECLASSIFICATION DOWNGRADING SCHEDULE

16. DISTRIBUTION STATEMENT (of this Report)

Approved for public release; distribution unlimited.

17. DISTRIBUTION STATEMENT (of the abstract entered in Block 20, if different from Report)

18. SUPPLEMENTARY NOTES

This work sponsored by the Defense Nuclear Agency under RDT&E RMSS Code B344079464 Y99QAXSB27707 H2590D.

19. KEY WORDS (Continue on reverse side if necessary and identify by block number)

Cementation Breakdown
Pore-Air Effects
Ground Motion

20. ABSTRACT (Continue on reverse side if necessary and identify by block number)

Cementation breakdown has been modeled and its influence on the single burst ground motion in a representative MX geology has been assessed. Its effect is confined to a late-time signal and even for the extreme models assumed it does not appear to be a significant factor in predicting peak values or frequency content. The pore-air effect has also been modeled and its influence in both the high explosive (HE) and nuclear multiple burst environments have been computed. For the high explosive case there is a low frequency motion that does appear to be associated with the pore-air effect. This motion would →

DD FORM 1 JAN 73 1473 EDITION OF 1 NOV 65 IS OBSOLETE

UNCLASSIFIED 373050

SECURITY CLASSIFICATION OF THIS PAGE (When Data Entered)

20. ABSTRACT (Continued)

not be predicted by superposition. For the nuclear case, the pore-air effect is small enough that superposition does seem to be approximately satisfied.

TABLE OF CONTENTS

LIST OF ILLUSTRATIONS

I. INTRODUCTION

Subsequent to the calculation of expected single burst ground motion environments for the MX land mobile basing concept, two unusual phenomena were identified in the mechanical behavior of the near-surface alluvial materials which could affect the validity of those calculations.

The first of these phenomena, termed cementation breakdown, refers to the breakdown of material structure due to initial loading and its effect on subsequent loading. The second, termed the pore-air effect, refers to the role of pore pressure in the air-filled voids in determining near-surface motion in a high explosive (HE) event.

In this report an assessment is made of the effect of these phenomena on the original MX ground motion calculations. This is done by constructing the simplest possible models of the phenomena and performing typical ground shock calculations with them. It was found in all cases that the single burst ground motion environment was not strongly affected, although the pore-air effect could be important in H.E. tests and, therefore, in analyzing and scaling H.E. data to the nuclear case. The cementation breakdown effects could be important for multiburst situations, but additional quantitative information concerning their nature would have to be obtained before such an assessment could be made.

II. MODELS OF CEMENTATION BREAKDOWN AND CALCULATIONS

The initial model representations of cementation breakdown were constructed on the basis of previous experience with similar materials. It was felt that if the effect of the breakdown proved very significant, additional quantitative information could be sought from subsequent experiments designed for that purpose. In order to allow for various possibilities in the manner in which the cementation breaks down, three modifications of the CAP model, Ref. [1], were formulated.

These models were evaluated by implementing them in several ground shock calculations. The site chosen was the MX revised baseline site, Ref. [2], with 100 ft water table. The site consists of 100 ft of dry sand, 500 ft of wet sand, 400 ft of weak rock and the remainder is bedrock. The dry sand has a loading wavespeed of 1500 ft/s and an unloading wavespeed of 3600 ft/s. The wet sand has a low shear strength (150 psi) and an unloading wavespeed of 7000 ft/s. The weak rock and bedrock have wavespeeds of 10,000 ft/s and 14,000 ft/s, respectively. In all the calculations the air blast load was provided by a 1 MT nuclear surface burst.

The three models studied were:

1) A degradation model - in which the failure envelope for dry and wet alluvia are monotonically reduced with decreasing range, from a non-degraded value to some smaller value in the vicinity of ground zero. This model attempts to represent, in a qualitative sense, the expected reduction in the shear strength of the material which results from the very severe loadings in the close-in region.

2) A damage model - in which the overburden material shows a reduction in shear strength that is directly related to compaction loading. In this model, the frictional effects associated with the failure surface at low pressures are monotonically reduced with continued plastic

compaction, thus weakening the material during its unloading-reloading cycle.

3) A compaction damage model - in which the uniaxial strain reloading modulus is reduced as a function of the amount of initial compaction for loading and the amount of unloading. This effect was obtained by modifying the hardening rule in the CAP model.

The degradation model, which is illustrated in Fig. 1, is obtained by multiplying the shear strengths of the dry and wet sands by a fractional factor which is a function of the range from ground zero. For the purposes of this study, the degraded shear strength was taken to be 10% of its original value at zero range, and increased linearly with range out to 2000 ft (~ 500 psi) as shown in Fig. 1, so that the overall failure envelope can be written as

$$\sqrt{J_2'} = [\min(1, .1 + \frac{.9}{2000} R)] F(J_1) \tag{1}$$

where $F(J_1)$ is the cap model failure envelope J_1 is the sum of the normal stresses J_2' is the second invariant of the stress deviator and R is the range from ground zero measured in feet. Equation (1) was assumed for both the dry and wet sand (alluvium) materials.

The damage model assumes that the dry and wet sands show a reduction of shear strength that is directly due to compaction loading. This material model, schematically illustrated in Fig. 2, uses both a limit surface to define the top of the cap, and a separate failure surface that extends from the tension-cutoff point to the top of the cap. By this mechanism, the friction angle associated with the failure surface at low pressure is monotonically reduced with continued plastic compaction. In this case the failure envelope can be written

$$\sqrt{J_2'} = \min[F(J_1), (\frac{J_1 - T}{L - T}) F(L)] \tag{2}$$

where T is the material tensile strength and L denotes the location of the top of the cap.

The effect of this damage model on the uniaxial behavior of the dry sand is given in Figs. 3 and 4. Naturally it is only the unloading-reloading behavior that is affected by the damage aspect of the model.

The third model, termed a Compaction Damage model, was formulated because the Waterways Experimental Station (WES) suggested that the main effect of breakdown of cementation may be reduced stiffness in reloading with no appreciable reduction in shear strength. The uniaxial laboratory data that was reported by WES, Ref. [3], is reproduced in Fig. 5. The data includes measurements for specimens that were taken from the testing machines, broken up, remolded and reloaded. Clearly, this is an extreme case of cementation breakdown. Therefore, it is expected that the modeling of this effect would provide a worst case representation of the in situ behavior under explosive loading.

The Compaction Damage model, is a modification of the soil cap model. In the original soil CAP model, Ref. [1], any loading which produces shear or tension failure results in a backward motion (and contraction) of the cap that is directly proportional to the dilatant strain.

Specifically, $\Delta\kappa = (\frac{d\kappa}{d\epsilon_v^p}) \Delta\epsilon_v^p$,

where κ is the cap parameter and $\Delta\epsilon_v^p$ is the (dilatant) plastic volume strain. Further, in the original CAP model, there is no distinction between loading

and reloading properties of the model. In particular, the locking strain, defined by W, remains unchanged.

To obtain the Compaction Damage model, two modifications were made to the soil cap model. First, the increment in κ as determined by $\Delta\varepsilon_v^p$ was multiplied by 100 in order to insure a rapid retraction of the cap under failure or tension. Secondly, the value of W (the locking strain) was incremented by $\Delta W = CZ * \Delta\varepsilon_v^p$ where CZ is a material damage coefficient. This increase in W gives a reduced reloading modulus (for low pressures the loading modulus is inversely proportional to W), which seems to be indicated by the WES data. The value of CZ was taken as 15 so that the dry sand studied would give a uniaxial loading, unloading and reloading behavior that is similar to that of the WES data. In Fig. 6 the uniaxial behavior of the dry sand model is shown.

It must be emphasized that the modified CAP model does not undergo any work-softening since the reduction in W only occurs on the failure envelope or in tension and not during any plastic compaction (i.e., loading on the cap). The model is therefore stable; it satisfies all the requisite conditions to be mathematically well-posed.

Ground shock calculations, as previously described, were performed with cementation breakdown models. Comparisons were then made with previous runs which did not include cementation breakdown effects (designated as WT 100).

First, the degradation and damage models were run. The velocities and displacements at the 600 psi range are compared in Figs. 7 - 10 with the original WT 100 calculation. As expected, it is the later time horizontal motions that display the greatest difference from the baseline case. Note that the damage calculation, because of the local reduction in shear strength does not exhibit the rebound in horizontal velocity and

corresponding reduction in the displacement. However, in both calculations, there does not appear to be any effect that would significantly alter the present revised baseline waveforms for this site and range.

As an illustration of the way these models are being exercised, several stress paths are also included. Figures 11 - 12 illustrate the degraded failure envelope below ground zero and at a range of 1080 ft in the wet sand layer. Figures 13 - 14 indicate the degree to which the failure surface has been damaged by the plastic compaction in the wet sand material.

The Compaction Damage model was evaluated in a similar way. Again, the revised baseline site was utilized, with the dry sand including the Compaction Damage model. The velocities and displacements at the 600 psi range are compared with the original WT 100 in Figs. 15 - 16. As expected, only the later motions display some difference from the baseline. As in the previous model, however, these differences are not large; there does not appear to be any significant effect of the modified reloading behavior on the amplitudes or frequency content of the resulting motions. In fact, comparisons out to the 100 psi range show the same order of difference as at the 600 psi range.

As an illustration of how the modified CAP model is being exercised the associated stress path and the history of W at the 600 psi range is given in Fig. 17 and Fig. 18. The large change in W occurs at about $t \approx .45$ sec (which corresponds to unloading on the failure envelope in Fig. 17). It is this change in W that gives the reduced reloading modulus. However, as can be seen from the stress path, there is only a limited amount of reloading on the cap.

In conclusion, the breakdown in cementation that is either modeled by a reduction in shear strength or a reduction of the reloading modulus does not significantly affect the ground shock response at the MAP site for single

bursts. The effect of such phenomena on multiple burst response is potentially much greater. A study of such effects, however, would require substantial quantitative data on how the materials actually break down so that the appropriate model can be used. Because the most recent tests, Ref. [4], show that cementation breakdown affects the mechanical behavior of alluvial materials less than originally suspected, these studies have been deferred.

III. PORE AIR MODEL

Pore air effects are potentially important in near surface ground motions resulting from near-surface explosions. As an example, it has been proposed, Ref. [5], that the later time, low frequency upward motions observed in the MISERS BLUFF series of single and multiple burst tests can be attributed to the pressure differential between air entrapped or compressed in the porous near-surface silt and the negative phase underpressure in the airblast loading on the ground surface.

To test this hypothesis, a model was constructed which could be easily used in existing ground shock codes. Although there is a wide range of models which could be used for this purpose, the model chosen represents a compromise between a complete two-phase approach and the simplicity required for the standard single-phase ground shock codes.

The model is based on the assumptions that:

1) during compaction the material behaves in the usual solid manner (CAP model)

2) that this solid behavior occurs when the pressure is greater than some history dependent threshold pressure (which represents the pressure of the entrapped, and possibly compressed, air)

3) for pressures below the threshold, the solid material "falls apart" and supports no stress, i.e., the equation of state of the air is used (adiabatic expansion and compression, with all strains taken by the air).

To complete the model, the threshold pressure must be defined. It is initially one atmosphere (absolute), but its subsequent behavior depends on the porosity of the material, the deformation history, and the extent to which pore-air migration is allowed. If complete migration is allowed, the

threshold pressure is constant. If no migration is permitted, then the air is compressed to an extent commensurate with the compaction of the solid.

The qualitative behavior of the model for hydrostatic loading is shown in Fig. 19 and the behavior in uniaxial strain is shown in Fig. 20 for a threshold pressure behavior which allows some migration of the pore air. The stress path corresponding to Fig. 20 is shown in Fig. 21.

This pore air model was used in a series of calculations of event MB I-4, in which six charges, each with a yield of one half ton, were detonated in a hexagonal array. In order to analyze the model near the center of the charge array, an axisymmetric soil island approximation to the event was made, as shown in Fig. 22. The radius of the island was chosen to be half the distance from the array center to each of the charges; therefore, measured velocity data could be applied to the cylindrical boundary to eliminate any errors which would be associated with the calculations of the ground response directly from the bursts. Surface airblast loading resulting from the Low Altitude Multiple Burst (LAMB) code was used on top of the island.

The result of these calculations indicate that the use of the pore-air model leads to a greatly improved agreement between calculation and data as shown in Fig. 23. Although this doesn't prove that pore-air effects are the cause of the failure of superposition to represent all of the data, it indicates that this is a plausible explanation.

If it is taken for granted that pore-air effects are important in MISERS BLUFF, the question arises as to their importance in the case of nuclear explosions. To assess this, a two burst calculation was performed using the pore-air model. As expected, the results were not dramatically affected by pore-air behavior in the nuclear case. As shown in Fig. 24, the comparison to the two burst case with superposition remains good even when pore air effects are included. The smaller second peak in the two burst

case than would be expected by superposition is due to the previous compaction of the near surface porous material under the first air slap.

IV. CONCLUSIONS

Cementation breakdown has been modeled and its influence on the single burst ground motion in a MAP type of environment has been assessed. Its effect is confined to a late time signal and even for the extreme models assumed it does not appear to be a significant factor in predicting peak values or frequency content. The pore air effect has also been modeled and its influence in both the high explosive (HE) and nuclear multiple burst environments have been computed. For the HE case there is a low frequency motion that does appear to be associated with the pore-air effect. This motion would not be predicted by superposition. For the nuclear case, the pore-air effect is small enough that superposition does seem to be approximately satisified.

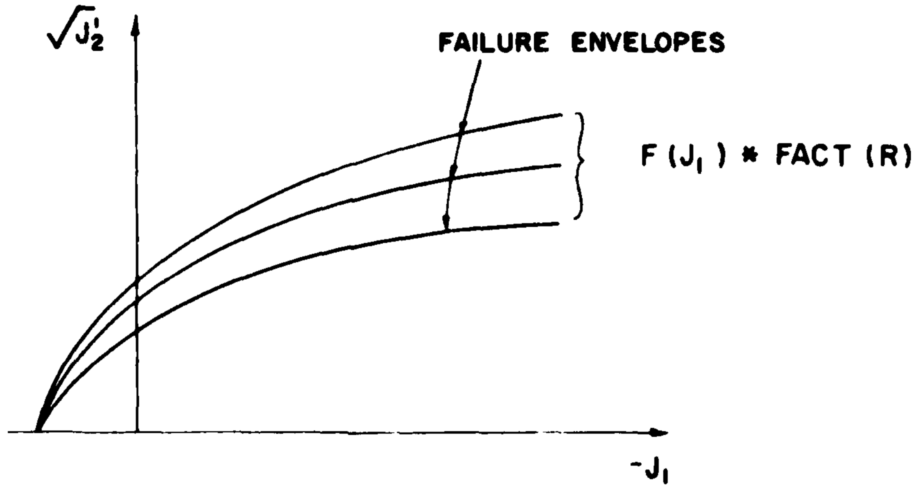

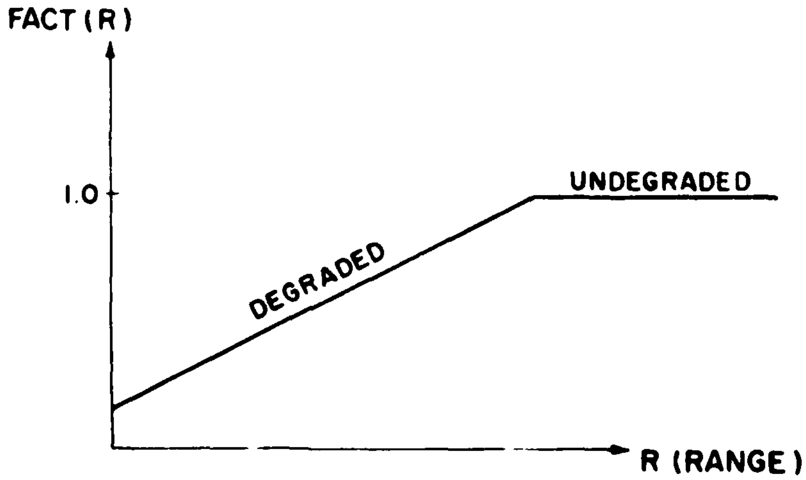

FIG. I DEGRADATION MODEL

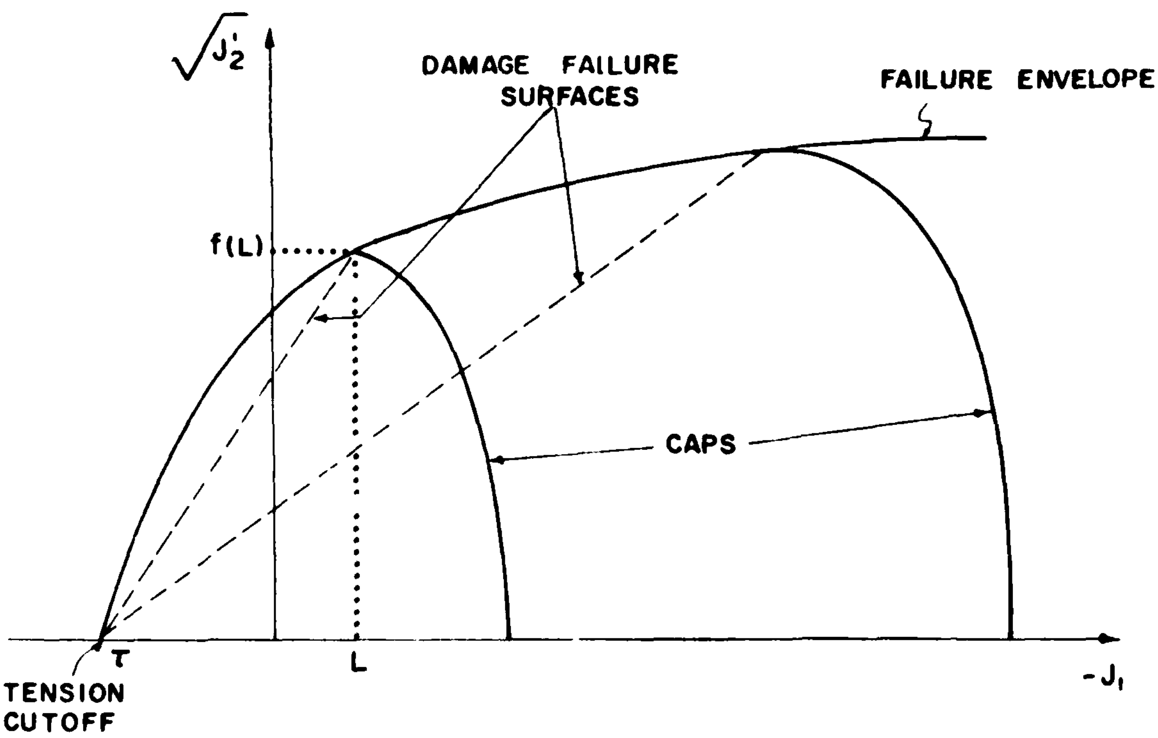

FIG. 2 DAMAGE MODEL

UNIAXIAL STRAIN TEST DRY SAND-1

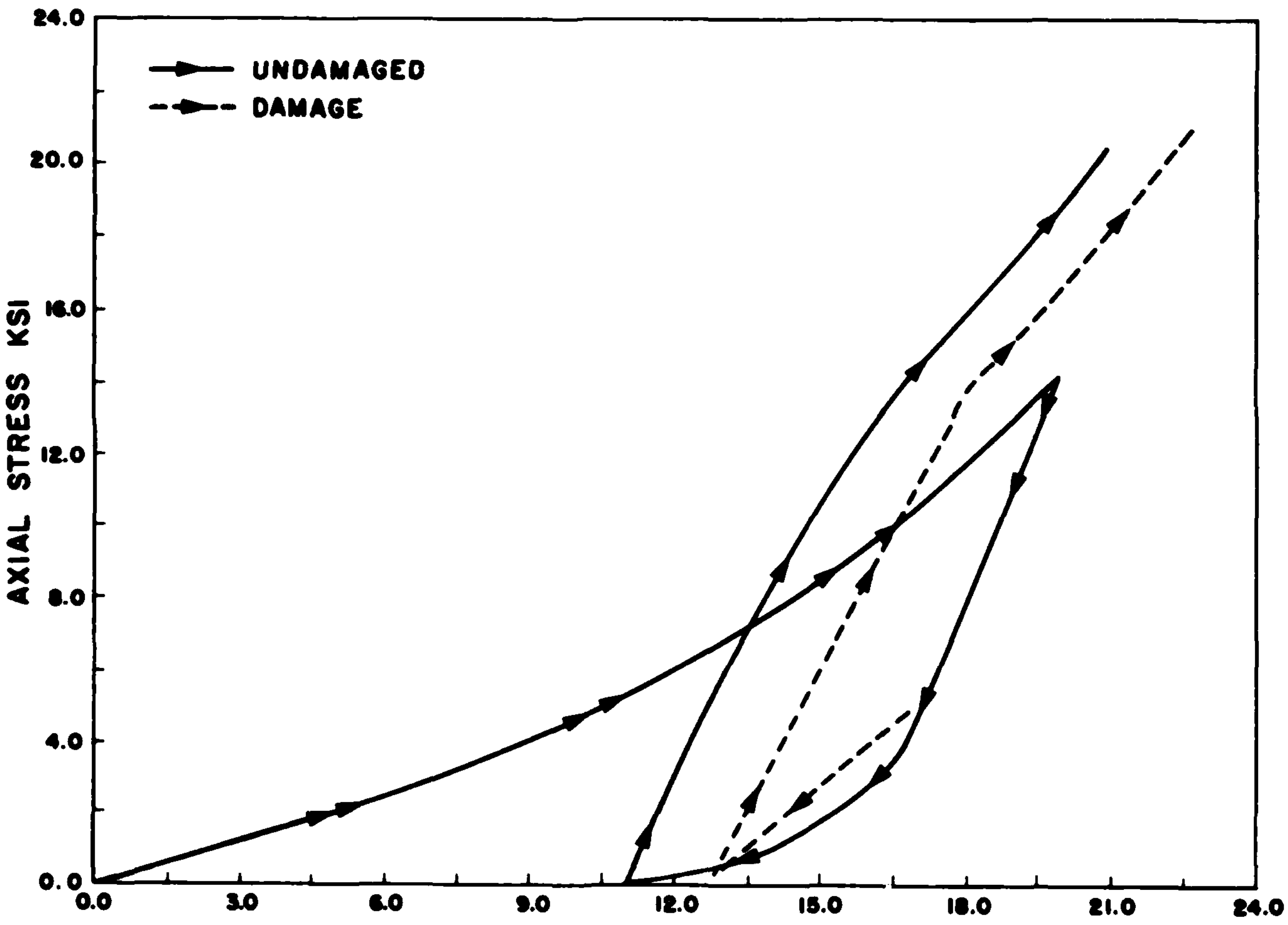

FIG. 3

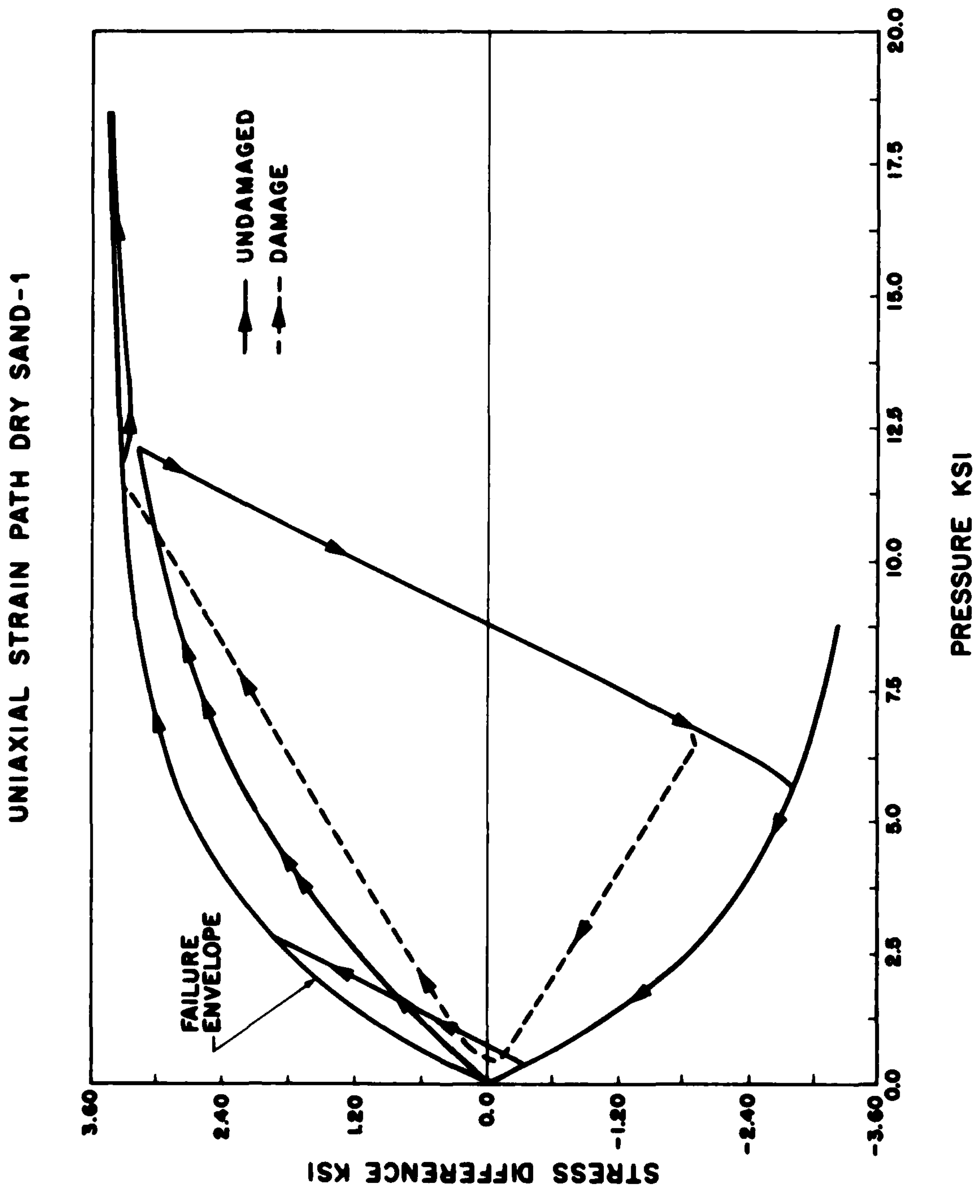

UNIAXIAL STRAIN PATH DRY SAND-1
UNDAMAGED
DAMAGE
FAILURE ENVELOPE
STRESS DIFFERENCE KSI
3.60
2.40
1.20
0.0
-1.20
-2.40
-3.60
0.0
2.5
5.0
7.5
10.0
12.5
15.0
17.5
20.0
PRESSURE KSI

FIG. 4

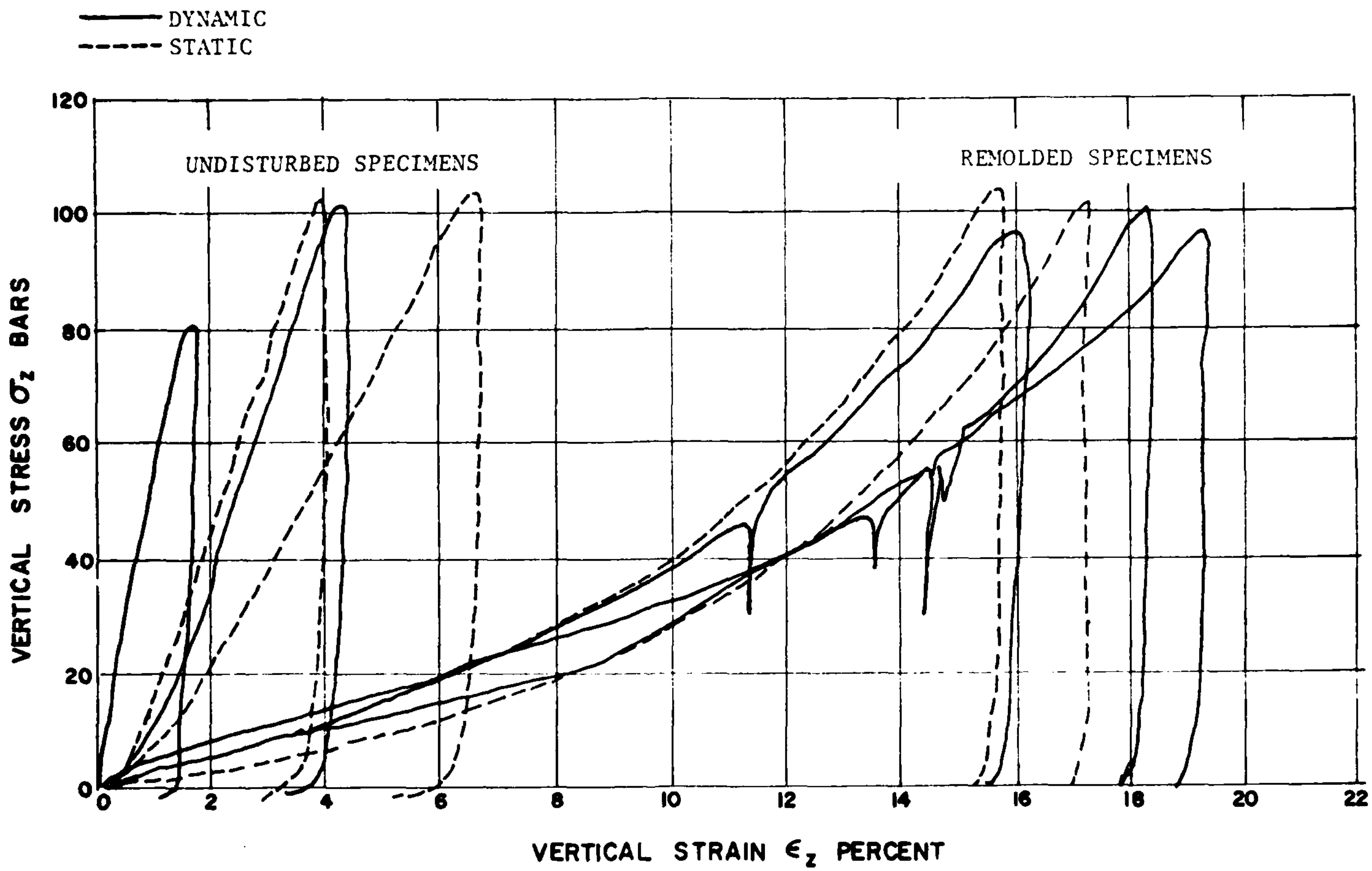

WES UNIAXIAL TEST RESULTS FOR CEMENTED SAND ALLUVIUM

FIG. 5

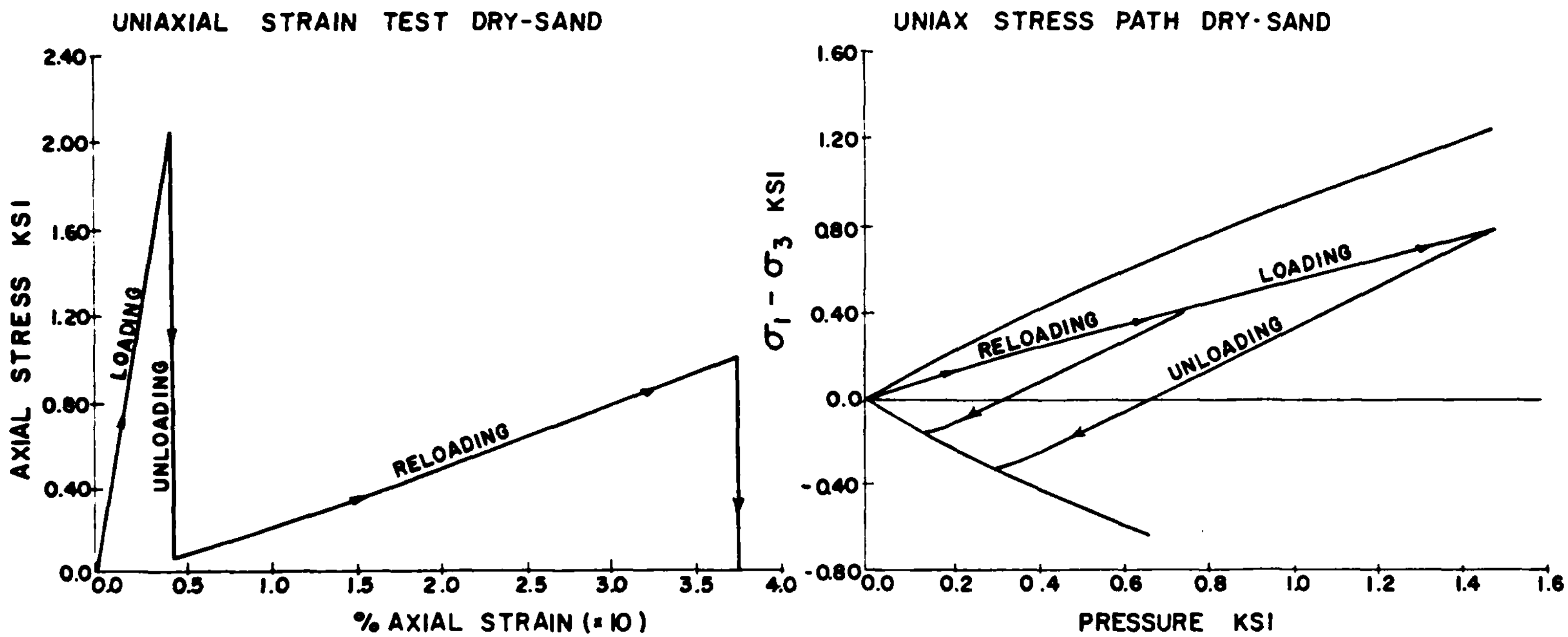

FIG. 6 UNIAXIAL BEHAVIOR OF DAMAGE MODEL

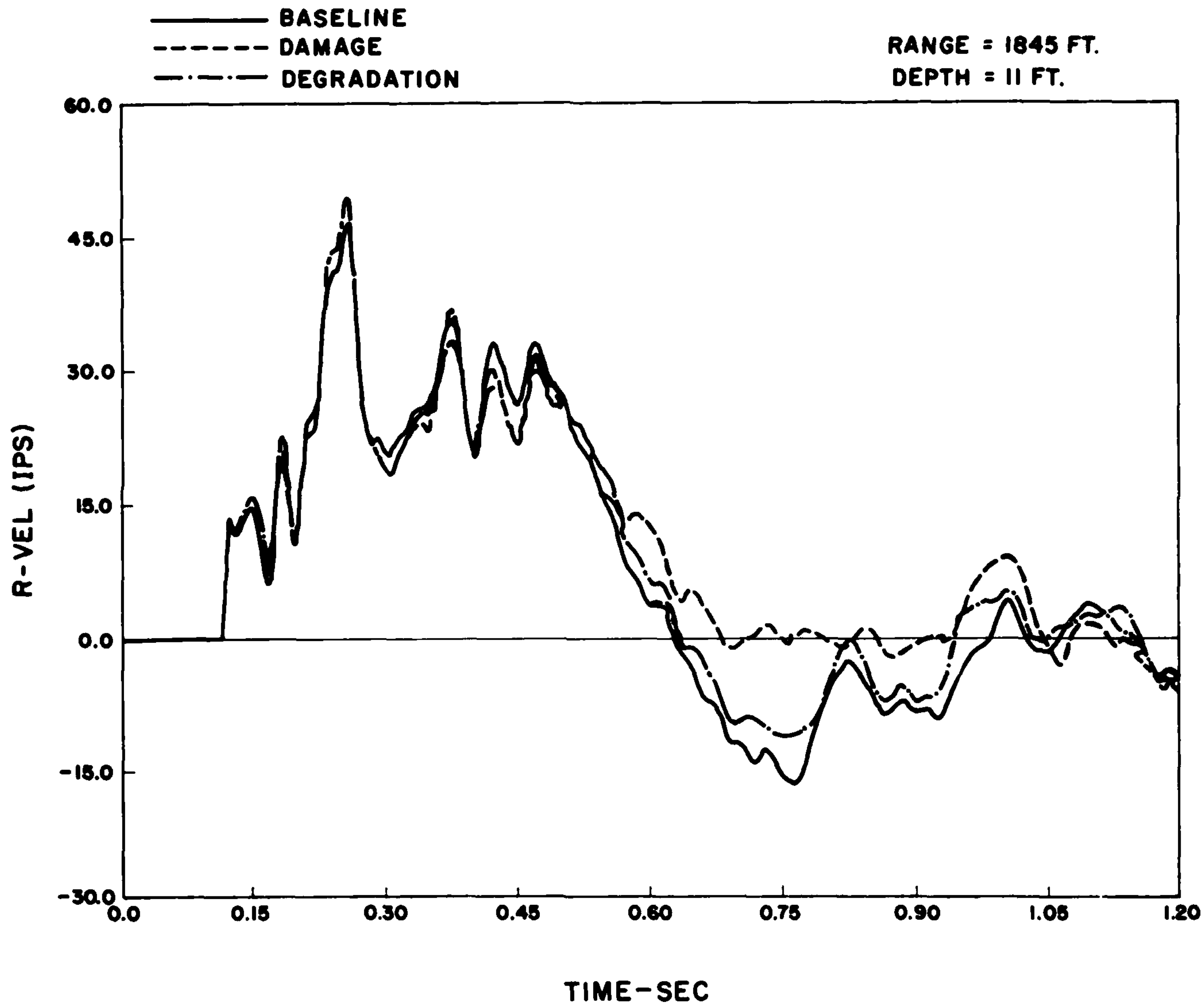

FIG. 7-HORIZONTAL VELOCITY-WT 100 COMPARISONS AT 600 PSI RANGE

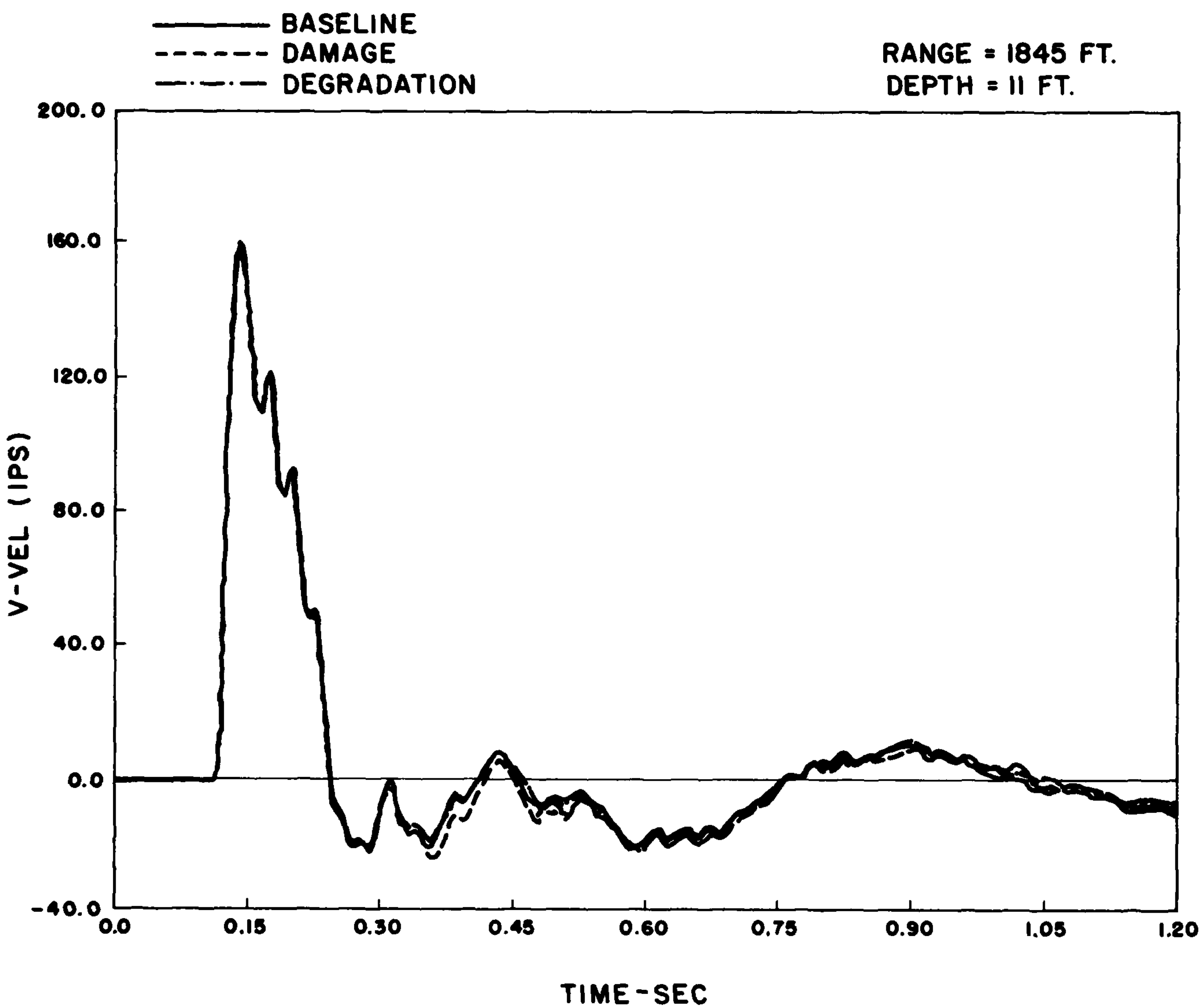

FIG.8 VERTICAL VELOCITY-WT 100 COMPARISONS AT 600 PSI RANGE

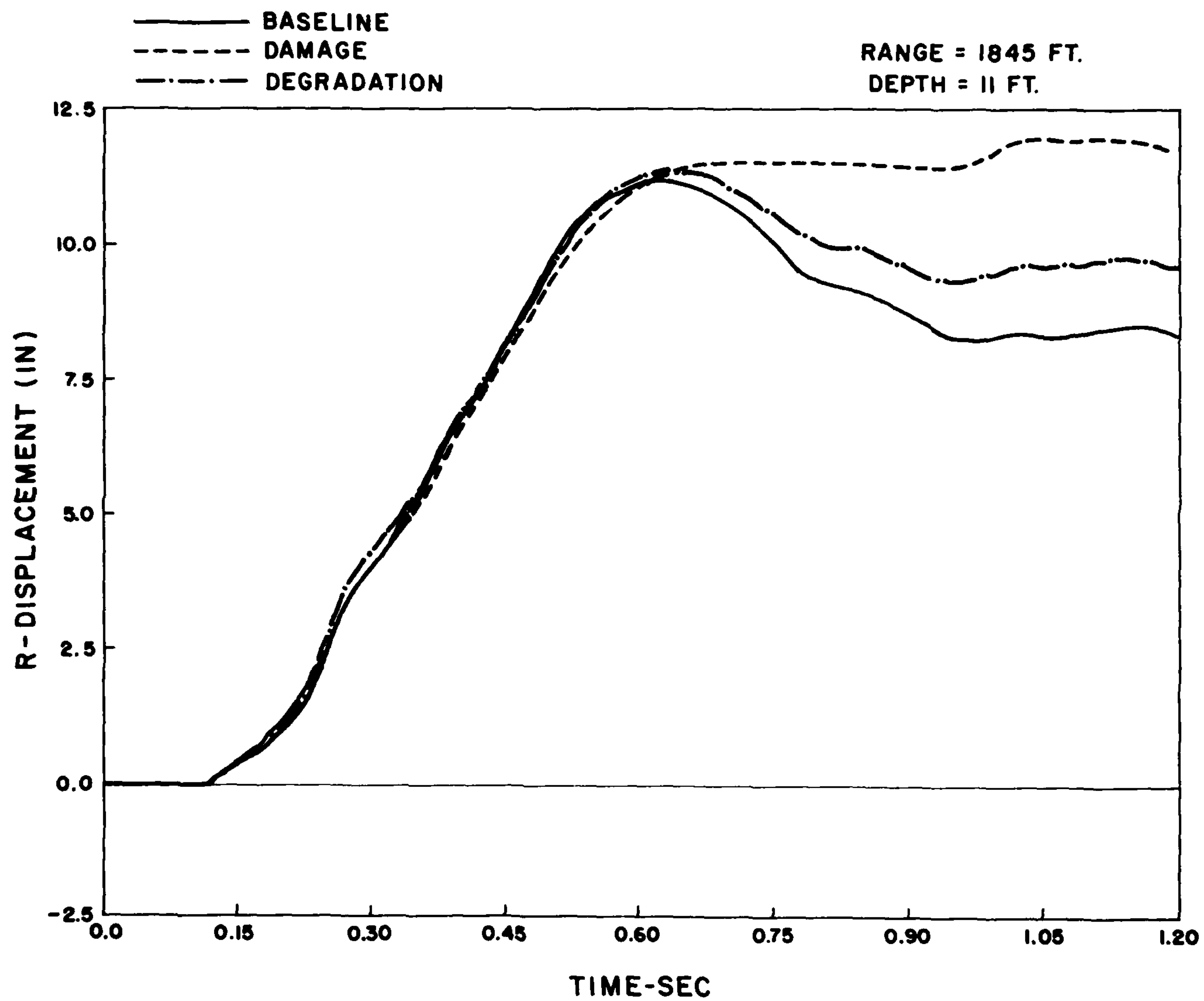

FIG. 9 - HORIZONTAL DISPLACEMENT-WT 100 COMPARISONS AT 600 PSI RANGE

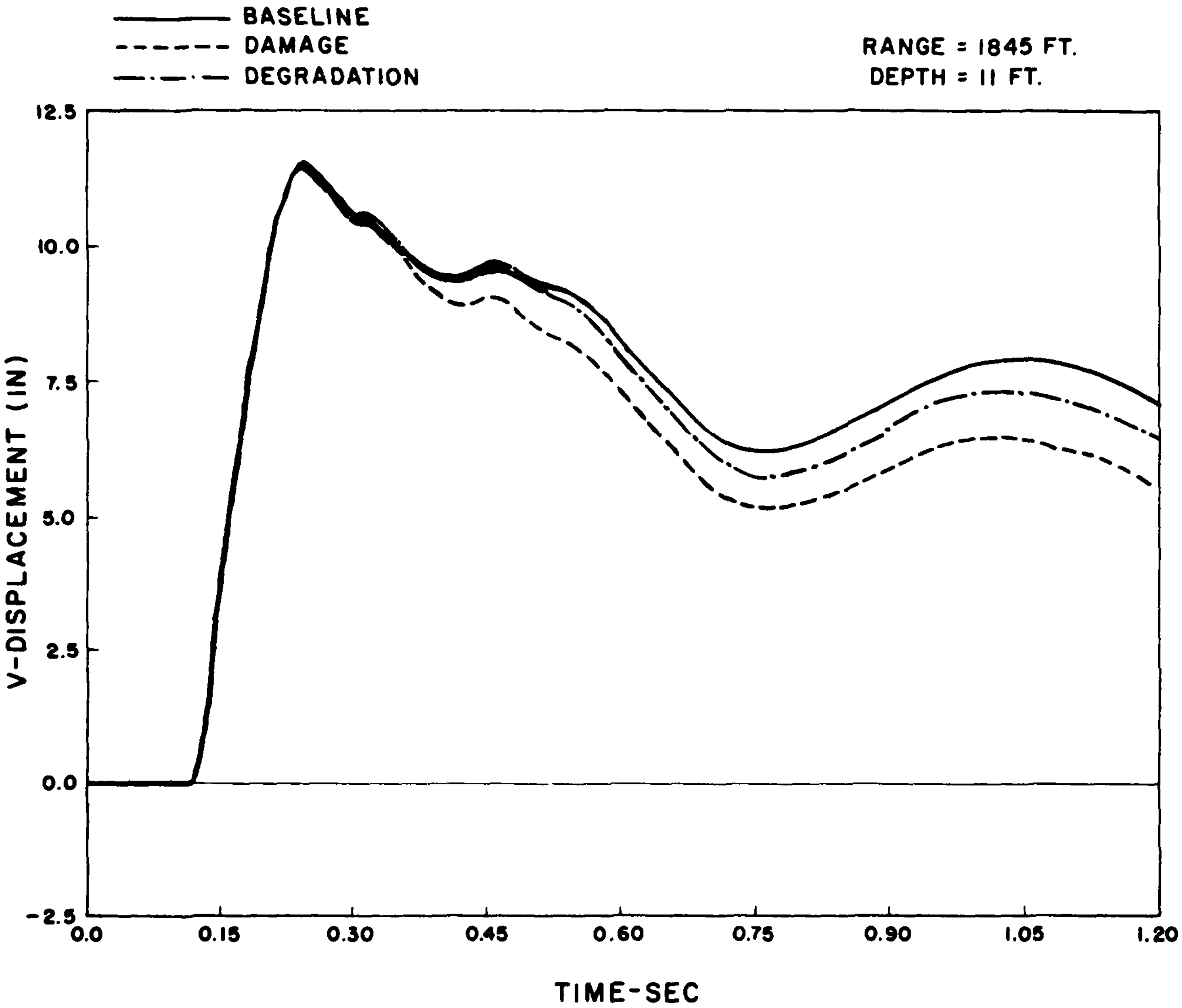

FIG. 10-VERTICAL DISPLACEMENT-WT 100 COMPARISONS AT 600 PSI RANGE

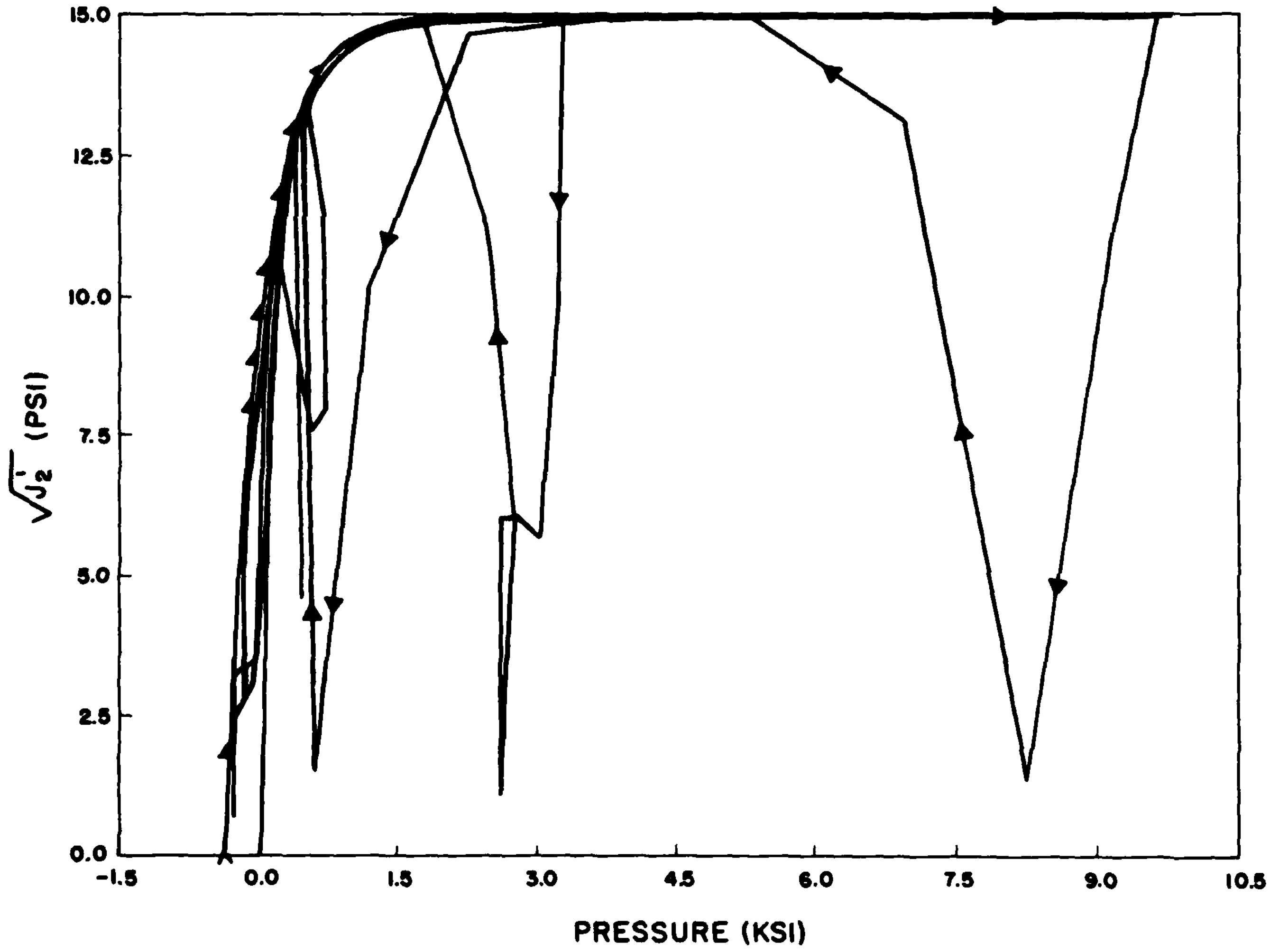

FIG. 11 STRESS PATH FOR DEGRADATION CALCULATION (450 FT. BELOW GROUND ZERO)

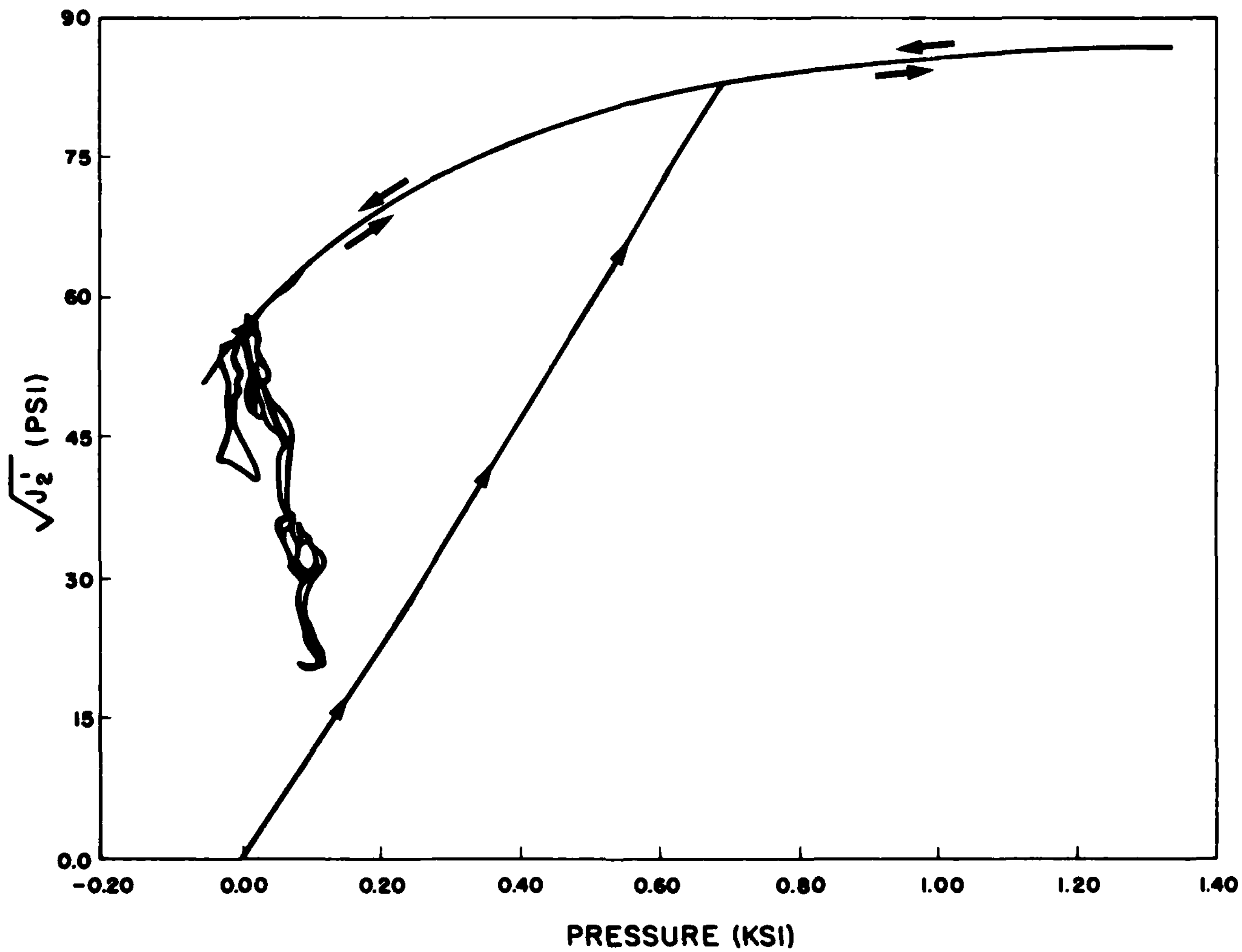

FIG. 12 STRESS PATH FOR DEGRADATION CALCULATION (R=1080 FT., Z = 450 FT.)

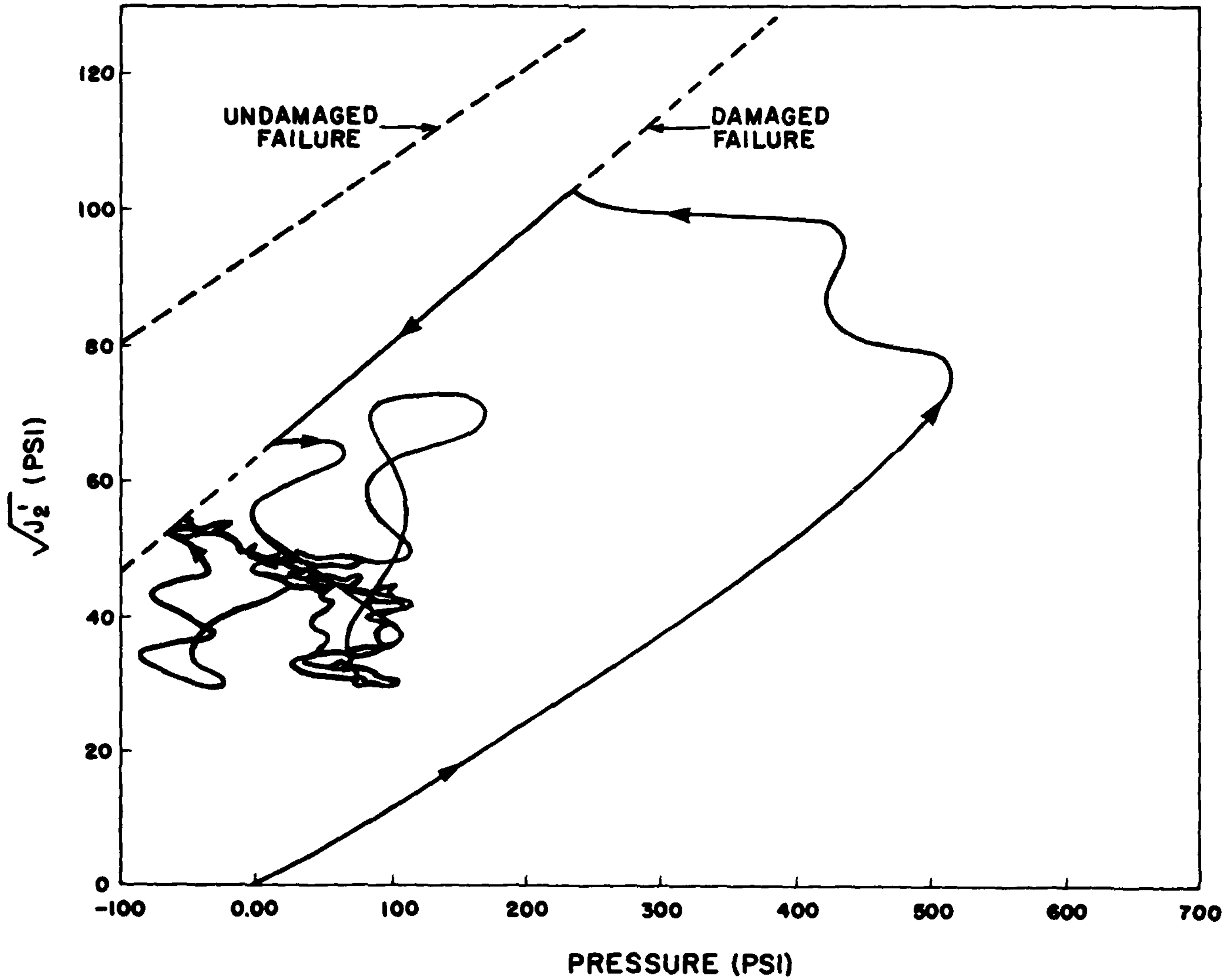

FIG. 13 STRESS PATH FOR DAMAGE CALCULATION (R = 1830 FT., Z = 450 FT.)

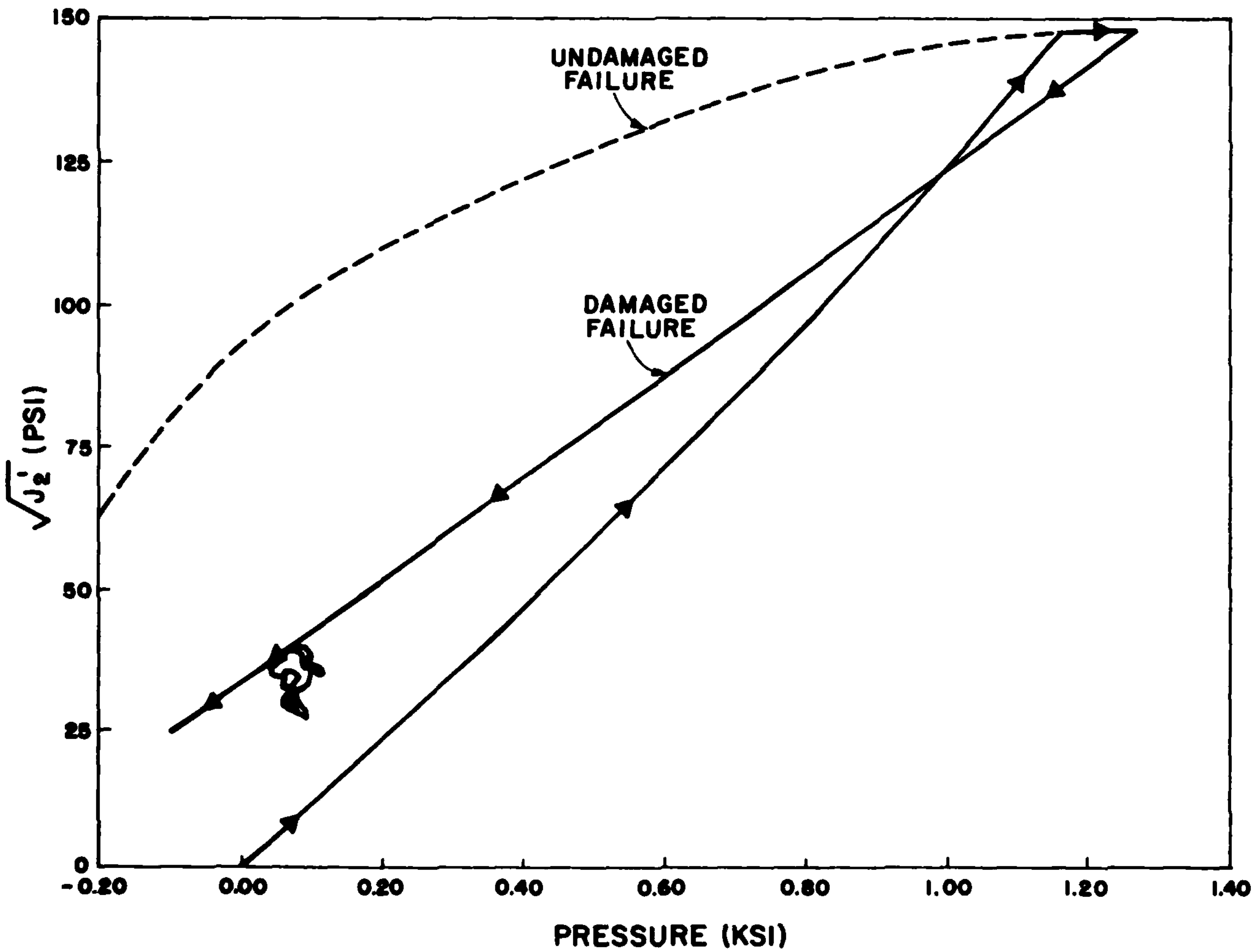

FIG. 14 STRESS PATH FOR DAMAGE CALCULATION (R = 1080 FT., Z = 450 FT.)

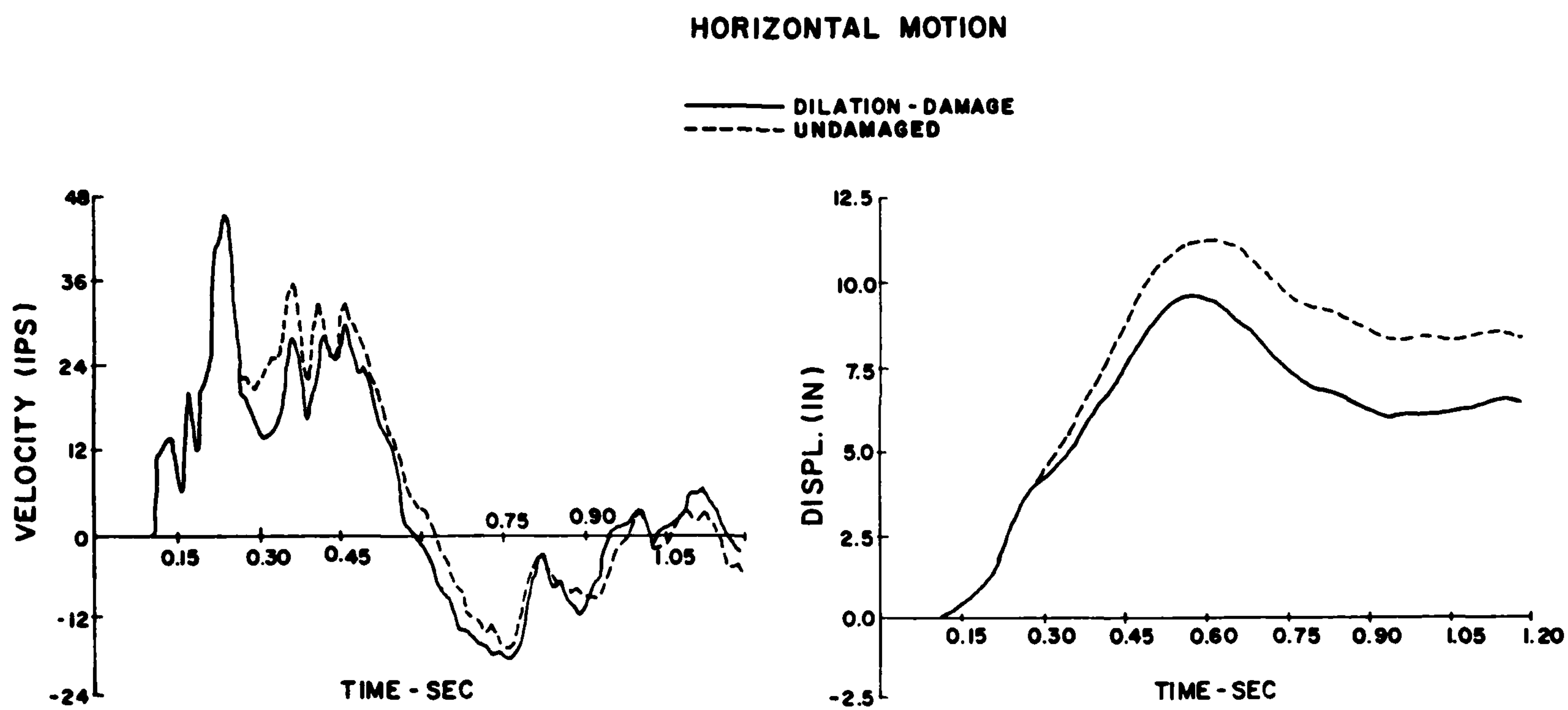

COMPARISON OF REVISED WT 100 BASELINE WITH COMPACTION
DAMAGE MODEL SITE AT 600 PSI
(R = 1845 FT., DEPTH = 11 FT.)

FIG. 15

VERTICAL MOTION

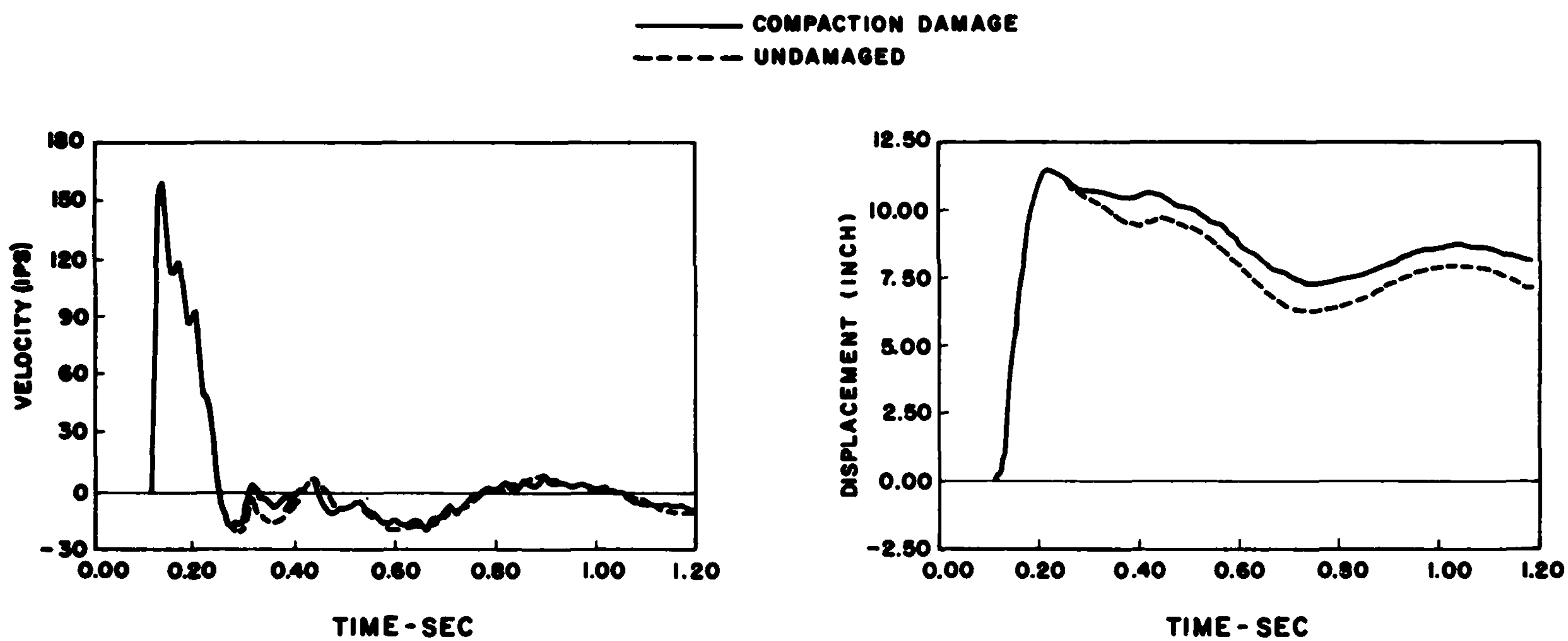

COMPARISON OF REVISED WT 100 BASELINE WITH COMPACTION DAMAGE MODEL SITE AT 600 PSI

(R = 1845 FT., Z = 11 FT.)

FIG. 16

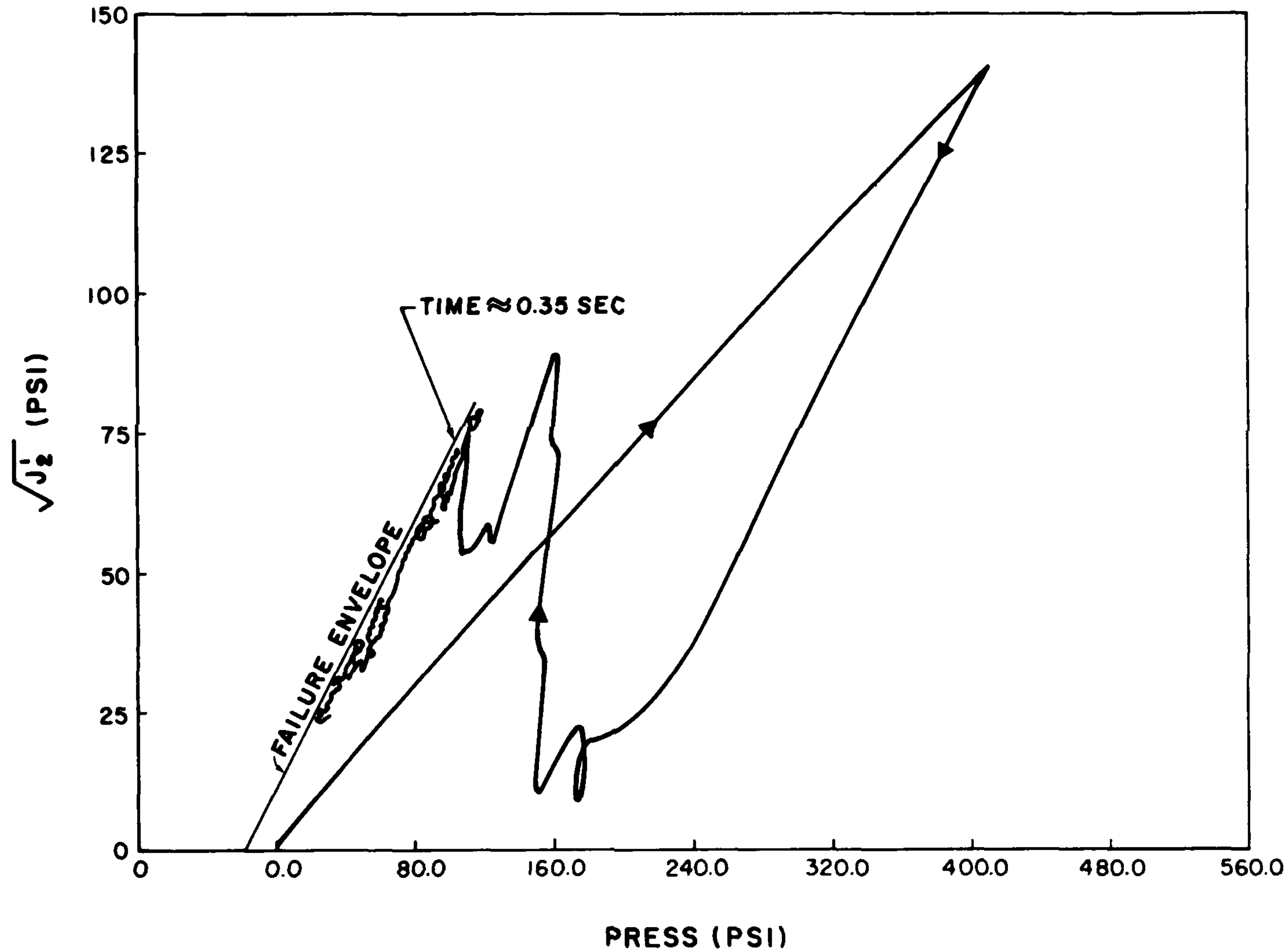

FIG. 17 STRESS PATH FOR COMPACTION DAMAGE CALCULATION (R=1803 FT, Z=0)

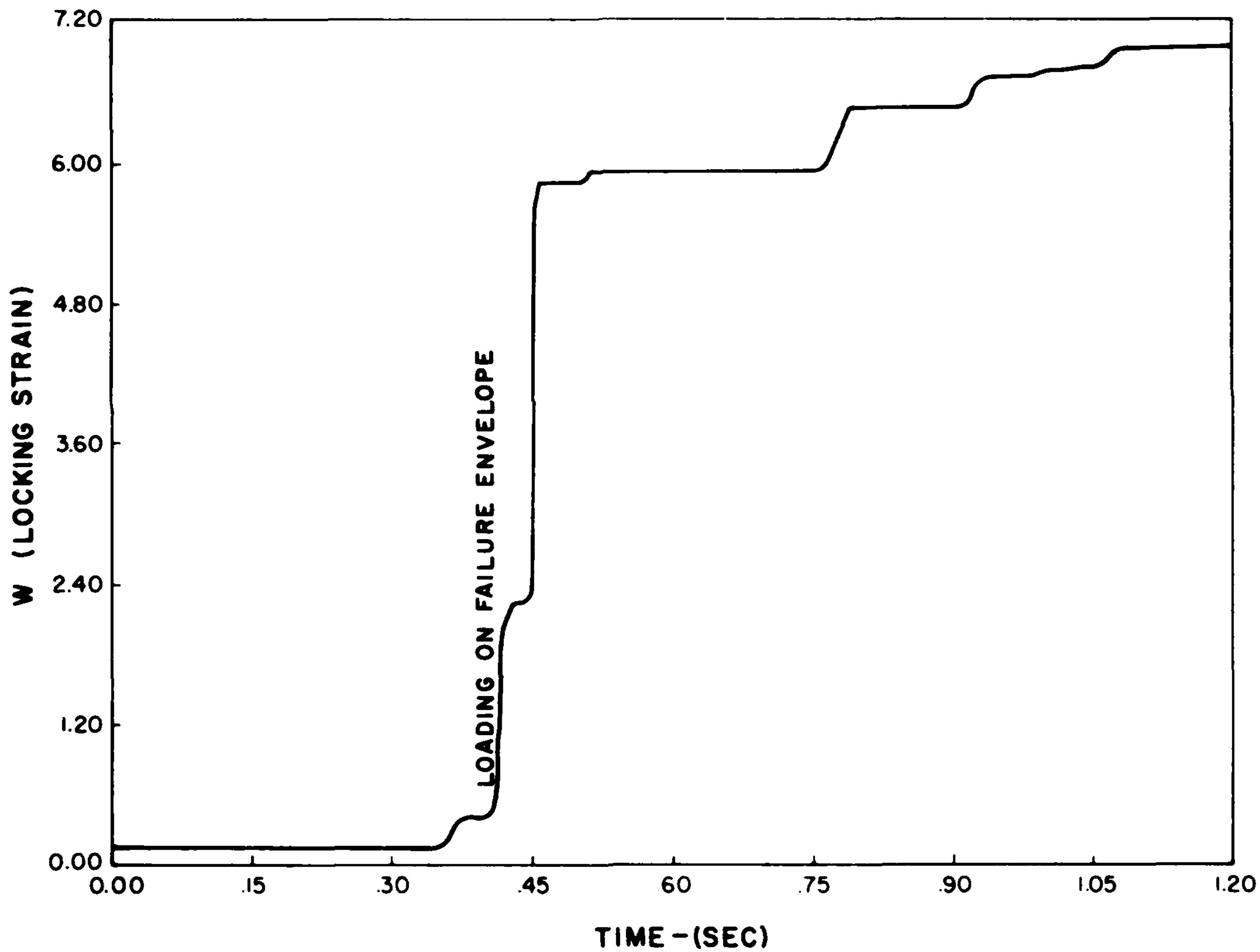

FIG. 18 HISTORY OF LOCKING STRAIN PARAMETER W FOR COMPACTION DAMAGE RUN

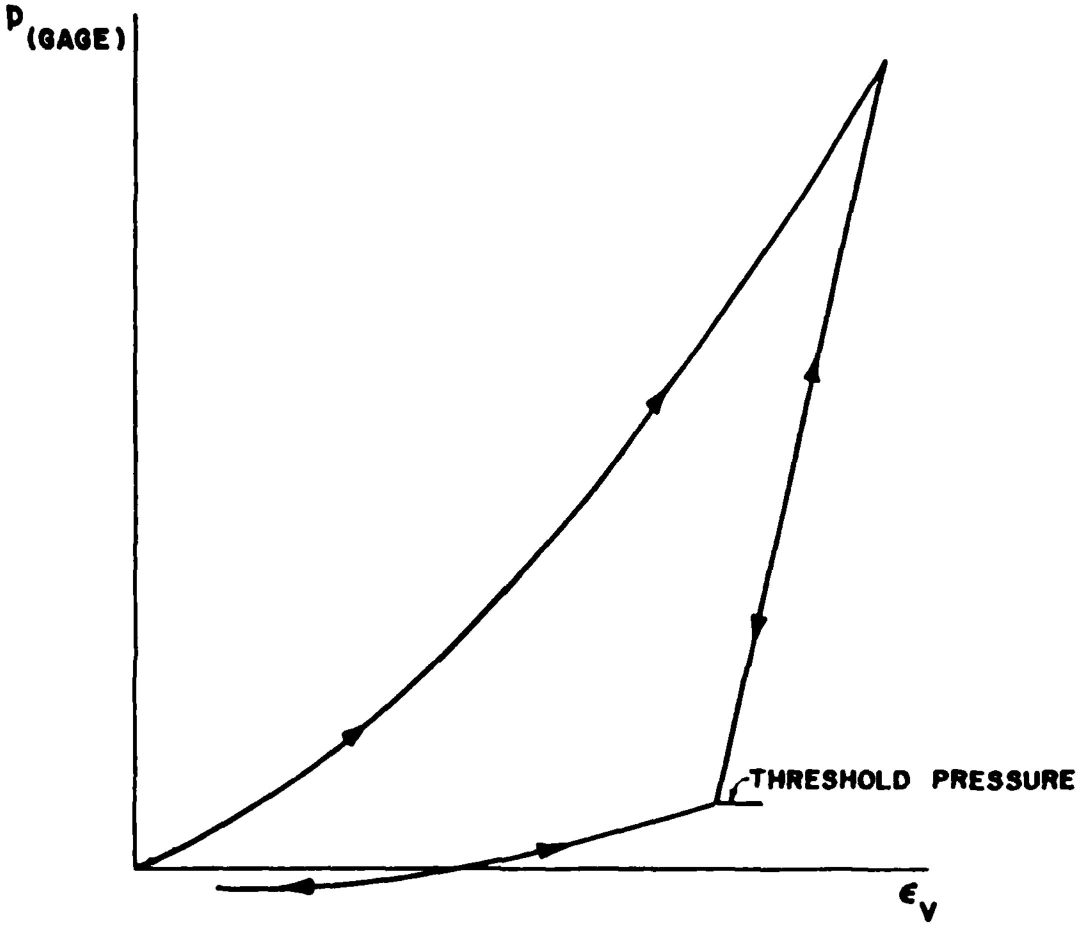

FIG. 19 HYDROSTATIC BEHAVIOR OF PORE AIR MODEL

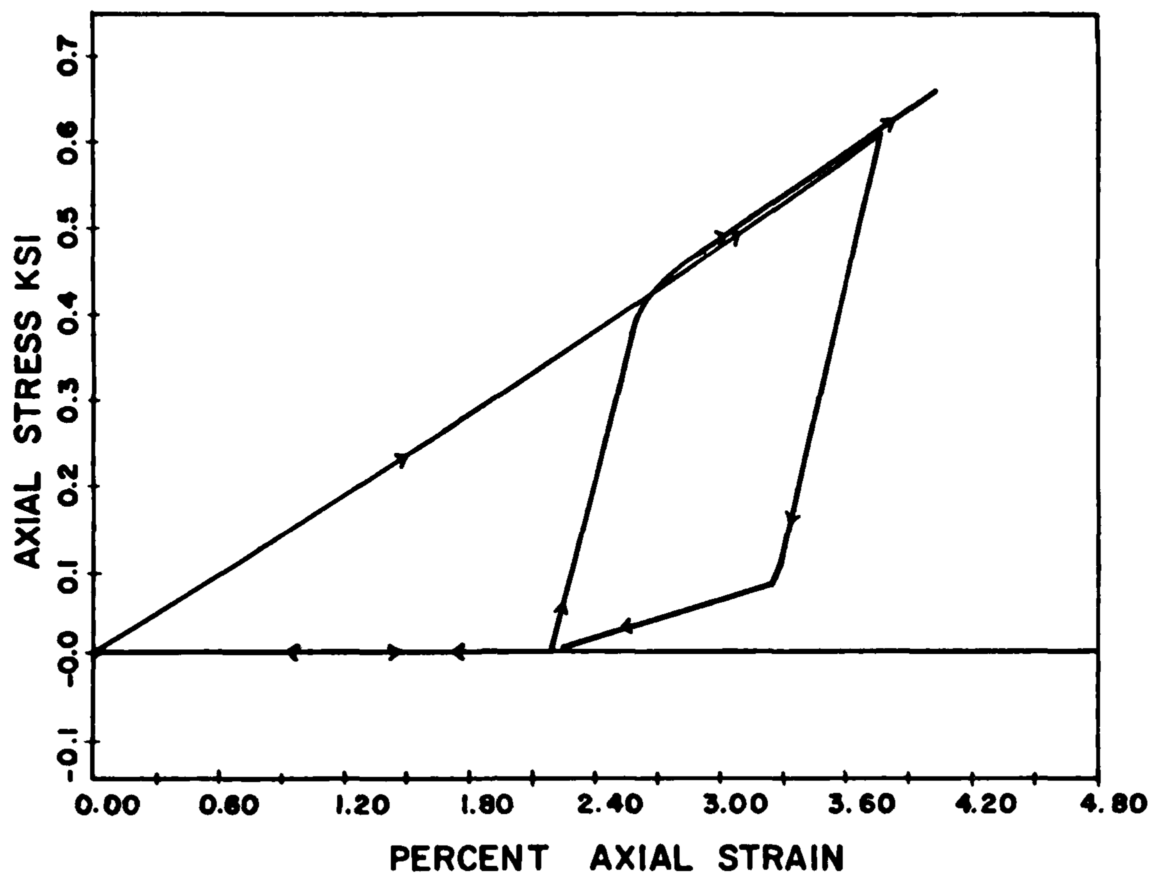

FIG. 20 UNIAXIAL BEHAVIOR OF PORE AIR MODEL

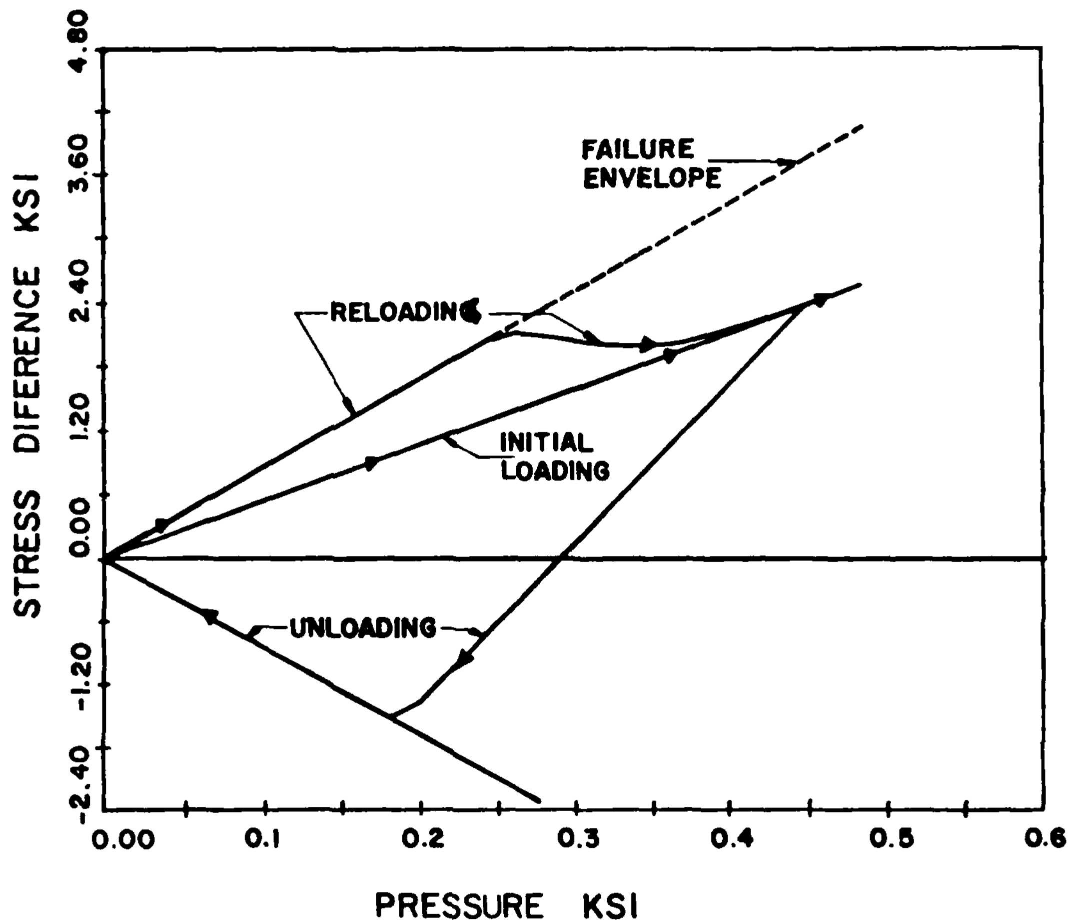

FIG. 21 STRESS PATH AND FAILURE ENVELOPE FOR PORE AIR MODEL

MISERS BLUFF CALCULATIONS

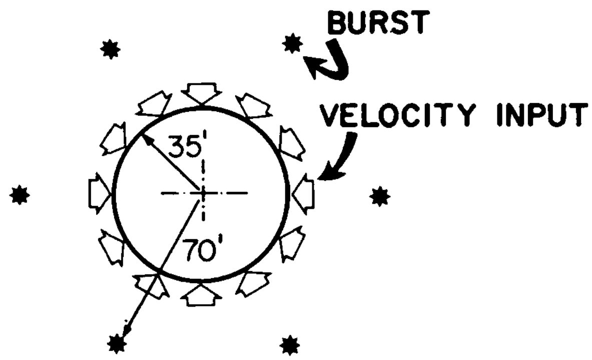

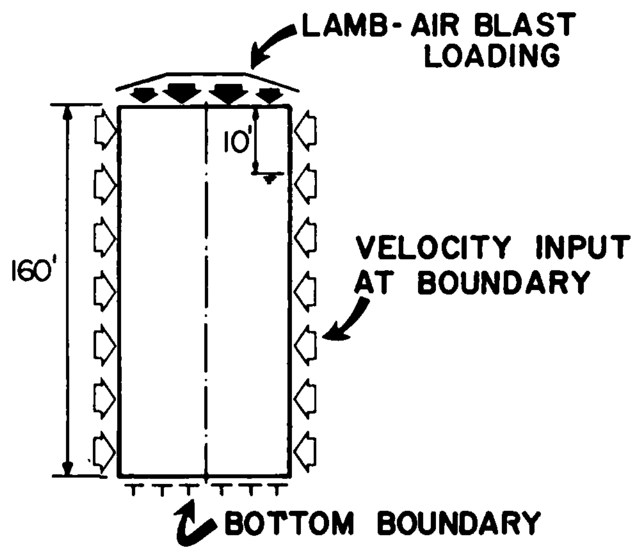

FIG. 22

COMPARISON OF STANDARD AND PORE AIR MODELS WITH MISERS BLUFF I-4 DATA (VERTICAL VELOCITY NEAR ARRAY CENTER)

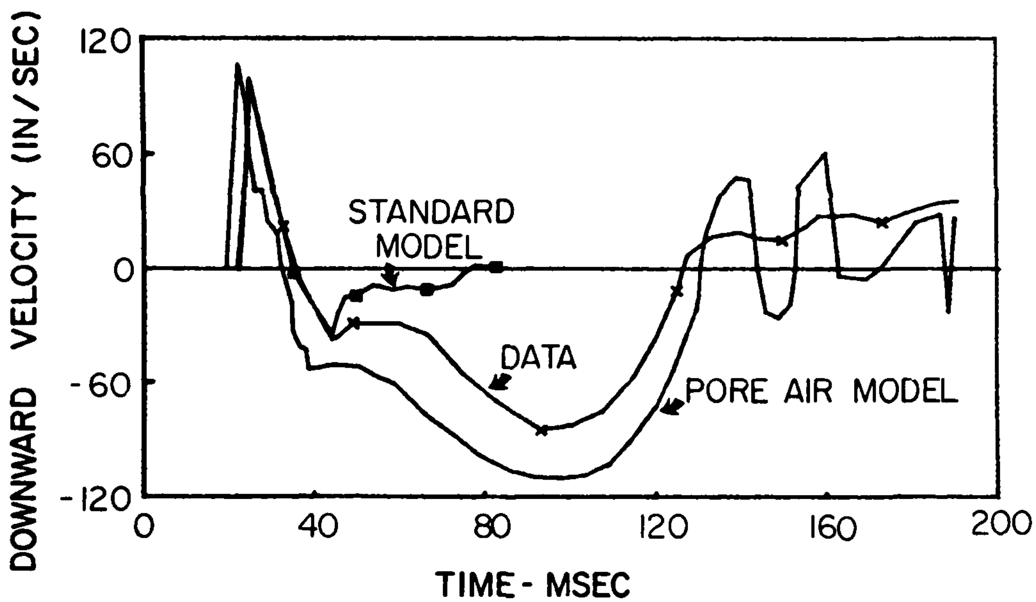

FIG. 23

CASE OF TWO SIMULTANEOUS NUCLEAR BURST (SPACING = 7400 FT., YIELD = 1 MT.) NEAR SURFACE VERTICAL MOTION 2400 FT. FROM BURST

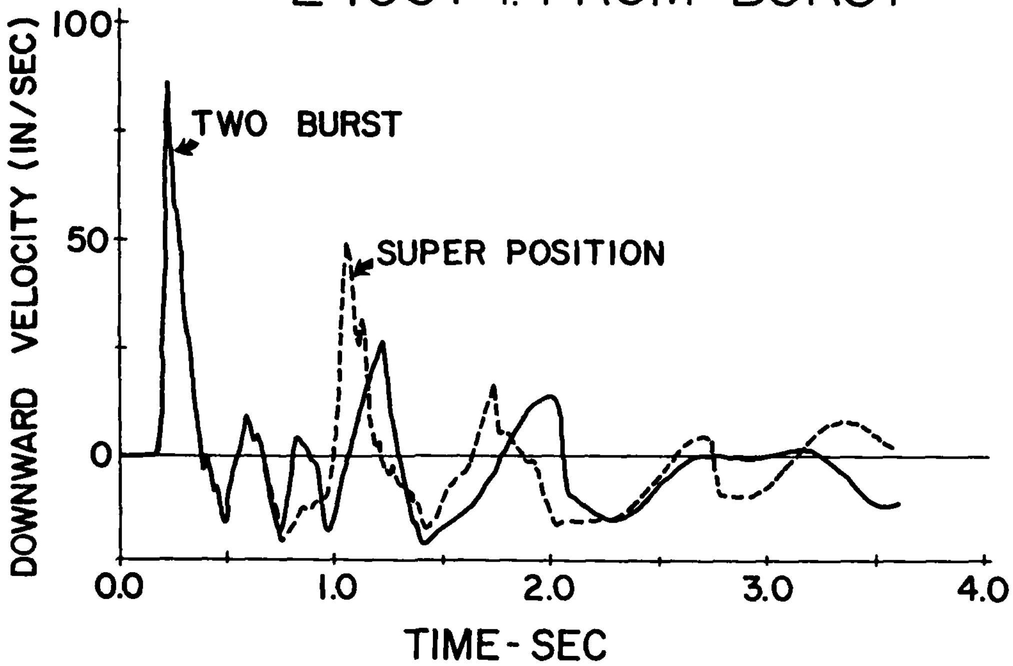

FIG. 24

REFERENCES

[1] Sandler, I.S. and Rubin, D., "An Algorithm and a Modular Subroutine for the Cap Model," Int. Jour. for Num. and Anal. Methods in Geomechanics, Vol. 3, 173-186 (1979).

[2] C-4 Progress Report No. 3, Weidlinger Associates, DNA001-77-C-0036, May 1977.

[3] Kontrim, B.J., "Laboratory Test Results for Cemented Sand Alluvium Obtained from Luke Bombing and Gunnery Range," Department of the Army, Waterways Experiment Station, Vicksburg, Mississppi 39180, DNA Subtask Y99QAXSX355, Work Unit 01, February 1977.

[4] Jackson, A.E., "Response Characteristics of LBGR Cemented Sand," Department of the Army, Waterways Experiment Station, Vicksburg, Mississippi 39180, DNA Subtask Y99QAXSX355, Work Unit 07, May 1979.

[5] Ullrich, G.W., "Airblast/Ground Motion Effects from Simultaneous Detonations of High Explosive Charges," Nuclear Technology Digest, AFWL-TR-78-110, Air Force Weapons Laboratory, Kirtland AFB, New Mexico, 1978.

DISTRIBUTION LIST

DEPARTMENT OF DEFENSE

Assistant to the Secretary of Defense
Atomic Energy
ATTN: Executive Assistant

Defense Advanced Rsch Proj Agency
ATTN: TIO

Defense Intelligence Agency
ATTN: RDS-3A

Defense Nuclear Agency
ATTN: SPSS, E. Sevin
ATTN: SPSS, G. Ullrich
3 cy ATTN: SPSS, J. Galloway
4 cy ATTN: TITL

Defense Technical Information Center
12 cy ATTN: DD

Field Command
Defense Nuclear Agency
ATTN: FCTMD
ATTN: FCPR

Field Command
Defense Nuclear Agency
ATTN: FCPRL

Joint Strat Tgt Planning Staff
ATTN: XPFS
ATTN: NRI-STINFO Library

Undersecretary of Def for Rsch & Engrg
Department of Defense
ATTN: Strategic & Space Systems (OS)

DEPARTMENT OF THE ARMY

BMD Advanced Technology Center
Department of the Army
ATTN: ATC-T

Chief of Engineers
Department of the Army
ATTN: DAEN-MPE-T, D. Reynolds
ATTN: DAEN-RDM
ATTN: DAEN-RDL
ATTN: DAEN-ASI-L

Harry Diamond Laboratories
Department of the Army
ATTN: DELHD-N-P
ATTN: DELHD-I-TL

U.S. Army Ballistic Research Labs
ATTN: DRDAR-TSB-S
ATTN: DRDAR-BLE, J. Keefer

U.S. Army Cold Region Res Engr Lab
ATTN: Library

U.S. Army Construction Engrg Res Lab
ATTN: Library

DEPARTMENT OF THE ARMY (Continued)

U.S. Army Engineer Center
ATTN: Technical Library

U.S. Army Engr Waterways Exper Station
ATTN: WESSD, J. Jackson
ATTN: Library
ATTN: WESSA, W. Flathau

U.S. Army Material & Mechanics Rsch Ctr
ATTN: Technical Library

U.S. Army Materiel Dev & Readiness Cmd
ATTN: DRXAM-TL

U.S. Army Nuclear & Chemical Agency
ATTN: Library

DEPARTMENT OF THE NAVY

Naval Construction Battalion Center
ATTN: Code L08A
ATTN: Code L51, J. Crawford
ATTN: Code L53, J. Forrest

Naval Facilities Engineering Command
ATTN: Code 09M22C

Naval Postgraduate School
ATTN: Code 0142 Library
ATTN: G. Lindsay

Naval Research Laboratory
ATTN: Code 2627

Naval Surface Weapons Center
ATTN: Code X211
ATTN: Code F31

Naval Surface Weapons Center
ATTN: Tech Library & Info Ser Br

Office of Naval Research
ATTN: Code 715

DEPARTMENT OF THE AIR FORCE

Air Force Institute of Technology
ATTN: Library

Headquarters
Air Force Systems Command
ATTN: DLWM

Air Force Weapons Laboratory
Air Force Systems Command
ATTN: NTE, M. Plamondon
ATTN: SUL
ATTN: NT, D. Payton
ATTN: NTED-I
ATTN: NTED-A
ATTN: DEY
ATTN: NTES-S
ATTN: NTES-G
ATTN: NTEO

DEPARTMENT OF THE AIR FORCE (Continued)

Assistant Chief of Staff
Intelligence
Department of the Air Force
ATTN: IN

Assistant Secretary of the Air Force
Research, Development, & Logistics
Department of the Air Force
ATTN: SAFALR/DEP for Strat & Space Sys

Ballistic Missile Office
Air Force Systems Command
ATTN: MNNX, W. Crabtree
ATTN: MNNXH, D. Gage

Deputy Chief of Staff
Research, Development, & Acq
Department of the Air Force
ATTN: AFRDQA
ATTN: AFRDPN
ATTN: AFRDQSM
ATTN: AFRD-P, N. Alexandrow

Strategic Air Command
Department of the Air Force
ATTN: NRI-STINFO Library
ATTN: XPFS

Vela Seismology Center
Department of the Air Force
ATTN: G. Ullrich

DEPARTMENT OF ENERGY CONTRACTORS

Lawrence Livermore National Laboratory
ATTN: D. Glenn

Los Alamos National Scientific Laboratory
ATTN: R. Sanford
ATTN: C. Keller

Sandia National Laboratories
ATTN: A. Chabai
ATTN: ORG 1250, W. Brown

OTHER GOVERNMENT

Federal Emergency Management Agency
ATTN: Hazard Eval & Vul Red Div

DEPARTMENT OF DEFENSE CONTRACTORS

Acurex Corp
ATTN: K. Triebes
ATTN: C. Wolf
ATTN: J. Stockton

Aerospace Corp
ATTN: Technical Information Services
ATTN: H. Mirels

Agbabian Associates
ATTN: M. Agbabian

Applied Theory, Inc
2 cy ATTN: J. Trulio

DEPARTMENT OF DEFENSE CONTRACTORS (Continued)

Boeing Co
ATTN: Aerospace Library
ATTN: S. Strack

California Research & Technology, Inc
ATTN: M. Rosenblatt
ATTN: Library

Civil Systems Inc
ATTN: J. Bratton
ATTN: S. Melzer

Eric H. Wang
Civil Engineering Rsch Fac
University of New Mexico
ATTN: J. Kovarna
ATTN: P. Lodde

General Electric Company—TEMPO
ATTN: DASIAC

H-Tech Labs, Inc
ATTN: B. Hartenbaum

Higgins, Auld & Associates
ATTN: H. Auld
ATTN: N. Higgins

IIT Research Institute
ATTN: Documents Library

J. H. Wiggins Co, Inc
ATTN: J. Collins

Merritt CASES, Inc
ATTN: Library

Mission Research Corp
ATTN: C. Longmire
ATTN: G. McCartor

Nathan M. Newmark Consult Eng Svcs
ATTN: W. Hall
ATTN: N. Newmark

Pacific-Sierra Research Corp
ATTN: H. Brode

Pacifica Technology
ATTN: R. Allen
ATTN: Library

Physics International Co
ATTN: Technical Library
ATTN: F. Sauer
ATTN: J. Thomsen

R & D Associates
ATTN: J. Lewis
ATTN: Technical Information Center
ATTN: C. MacDonald
ATTN: R. Port
ATTN: J. Carpenter
ATTN: P. Haas

DEPARTMENT OF DEFENSE CONTRACTORS (Continued)

R & D Associates
ATTN: A. Kuhl

Science Applications, Inc
ATTN: R. Schlaug
ATTN: Technical Library
ATTN: H. Wilson

Science Applications, Inc
ATTN: D. Houe

Science Applications, Inc
ATTN: B. Chambers III

SRI International
ATTN: D. Johnson
ATTN: J. Colton
ATTN: G. Abrahamson
ATTN: Library

Systems, Science & Software Inc
ATTN: C. Needham

Systems, Science & Software Inc
ATTN: J. Murphy

DEPARTMENT OF DEFENSE CONTRACTORS (Continued)

Systems, Science & Software Inc
ATTN: Library
ATTN: K. Pyatt
ATTN: C. Dismukes

Systems, Science & Software Inc
ATTN: C. Hastings

Terra Tek, Inc
ATTN: A. Abou-Sayed
ATTN: Library

TRW Defense & Space Sys Group
ATTN: Technical Information Cent
ATTN: N. Lipner

TRW Defense & Space Sys Group
ATTN: G. Hulcher

Weidlinger Assoc, Consulting Engineer
ATTN: I. Sandler

Weidlinger Assoc, Consulting Engineer
ATTN: J. Isenberg

DATE
FILMED

- 8